Third International Conference on Inverse Design Concepts and Optimization in Engineering Sciences
(ICIDES-III), Editor: G.S. Dulikravich, Washington D.C., October 23-25, 1991

Aerodynamic Shape Optimization of Arbitrary Hypersonic Vehicles

George S. Dulikravich and Scott G. Sheffer
Department of Aerospace Engineering
The Pennsylvania State University
University Park, PA 16802, USA

Abstract

A new method has been developed to optimize, in terms of aerodynamic wave drag minimization, arbitrary (nonaxisymmetric) hypersonic vehicles in modified Newtonian flow, while maintaining the initial volume and length of the vehicle. This new method utilized either a surface fitted Fourier series to represent the vehicle's geometry or an independent point-motion algorithm. In either case, the coefficients of the Fourier series or the spatial locations of the points defining each cross section were varied and a numerical optimization algorithm based on a quasi-Newton gradient search concept was used to determine the new optimal configuration. Results indicate a significant decrease in aerodynamic wave drag for simple and complex geometries at relatively low CPU costs. In the case of a cone, the results agreed well with known analytical optimum ogive shapes. The procedure is capable of accepting more complex flow field analysis codes.

Nomenclature

C_p	= surface pressure coefficient
C_{po}	= stagnation pressure coefficient
p	= static pressure at a point
p_∞	= free stream static pressure
M_∞	= free stream Mach number
θ_n	= angle between free stream and normal to the surface of a vehicle
A_m, B_m	= coefficients of Fourier trigonometric series for coordinates at cross section i
x	= Cartesian coordinate along the axis of the body
y, z	= Cartesian coordinates of a contour point at cross section i
s	= body cross section contour-following coordinate
$\bar{s}$	= normalized body cross section contour-following coordinate
γ	= specific heat ratio of the gas
A	= area of a panel on the body surface
$\bar{F}$	= aerodynamic force applied to a panel
$\hat{n}$	= unit normal to the body surface
M	= number of terms in the Fourier trigonometric series
S	= least squares summation
FAC	= percentage change in design variable

Subscripts

i	= i^{th} cross section of the vehicle
j	= j^{th} point of a cross section contour
m	= m^{th} coefficient of a Fourier trigonometric series
n	= angle between free stream and local body surface normal
∞	= free stream value

Introduction

Although optimization of axisymmetric hypersonic bodies has been accomplished in the past [1,2], the aerodynamic drag minimization of an arbitrary hypersonic vehicle has not been attempted [3]. The objective of this paper is to present an optimization procedure for arbitrarily shaped hypersonic vehicles. While there are certainly some limitations in this paper, including the choice of flow field solver and non-convergence for some shapes, it demonstrates that optimization of numerous variables can indeed be done and that this can be applied to complex configurations.

In hypersonic flow ($M_\infty > 5.0$), the flow around an object may be modeled using an impact theory. In this theory, oncoming particles strike, or impact, the surface of the object and impart the normal component of their momentum to that body. Classical Newtonian theory has been shown to approach reality when the free stream Mach number approaches infinity and the value of the ratio of specific heats approaches $\gamma = 1$ [4]. In the case of lower hypersonic Mach numbers, modified Newtonian theory has been shown to be quite satisfactory for predicting the aerodynamic forces and moments on a body [5]. Modified Newtonian theory has the main advantage of being extremely simple, accurate [6], and fast when faced with the thousands of flow field calculations needed in an optimization problem of this scope. Because of the use of modified Newtonian theory, it was implicitly assumed that the flow field was inviscid.

In this study, modified Newtonian impact flow theory was used with a modified Newtonian constrained search optimization routine [7] to obtain vehicle shapes which had significantly lower wave drag in inviscid hypersonic flow. In the first part of the study, cross section coordinates of the body were represented with curve-fitted Fourier series. Curve-fitted Chebyshev series [8] were initially considered, but it was found that the Fourier series represented complex shapes, such as a Space Shuttle configuration, better than the Chebyshev series. The coefficients of the Fourier series, one set representing the y coordinate and one set for the z coordinate (Fig. 1), then became the design variables that were fed to the optimization routine. The optimization routine sequentially perturbed each of the coefficients by a small amount and determined the new shape that reduced wave drag while keeping the volume and length of the vehicle constant. In the second part of the study, the y and z coordinates of the vehicle's cross section were used as the design variables directly. Again, the optimization routine perturbed separately each of the coordinates at each of the cross section contour points. Then, it combined the changes into a new shape with lower wave drag while still honoring the constraints of constant volume and constant length of the vehicle.

Numerical Models

The first part of this investigation used a least squares Fourier series curve fit to represent the y and z coordinates of each half cross section, i , that is,

$$y_{ij} = \sum_{m=1}^{M} A_{mi} \cos[(m-1)\pi \bar{s}_{i,j}] \qquad (1)$$

$$z_{ij} = \sum_{m=1}^{M} B_{mi} \sin[m\pi \bar{s}_{i,j}] \tag{2}$$

where $\bar{s}_{i,j}$ is a normalized contour-following coordinate (Fig. 1) such that

$$s_{i,j} = s_{i,j-1} + \sqrt{(y_{i,j}-y_{i,j-1})^2 + (z_{i,j}-z_{i,j-1})^2} \quad \text{and} \quad \bar{s}_{i,j} = \frac{s_{i,j}}{s_{i,jmax}} \tag{3}$$

and A_{mi} is determined from the least squares fit of the Fourier series

$$S_i = \sum_{j=1}^{jmax} \left(\sum_{m=1}^{M} (A_{mi} \cos[(m-1)\pi \bar{s}_{i,j}]) - y_{i,j} \right)^2 \quad \text{and} \quad \frac{\partial S_i}{\partial A_{mi}} = 0. \tag{4}$$

The coefficients B_{mi} are determined in a similar way. Since it was assumed that the vehicle had a vertical plane of symmetry, the z-coordinates of the first (j=1) and the last (j=jmax) point of each half cross section were always zero thus ensuring symmetry across the y-axis.

The local surface pressure coefficient, $C_{p,ij}$, was calculated by the use of modified Newtonian impact flow theory, which states that

$$C_{p,ij} = C_{po} \cos^2\theta_{n,ij} \tag{5}$$

where $\theta_{n,ij}$ is the angle between the free stream and the normal to the surface. The stagnation pressure coefficient, C_{po}, is given by

$$C_{po} = \frac{2}{\gamma M_\infty^2} \left[\left(\frac{\gamma + 1}{2\gamma M_\infty^2 - \gamma + 1} \right)^{\frac{1}{\gamma-1}} \left(\frac{\gamma+1}{2} M_\infty^2 \right)^{\frac{\gamma}{\gamma-1}} - 1 \right]. \tag{6}$$

The pressure on a given segment of the body may then be calculated from the rearranged formula for $C_{p,ij}$, that is

$$p_{ij} = p_\infty + \frac{1}{2} C_{p,ij} \gamma p_\infty M_\infty^2 \tag{7}$$

The aerodynamic force on each surface panel is found by

$$\bar{F}_{ij} = - p_{ij} A_{ij} \hat{n}_{ij} . \tag{8}$$

so that the resultant force is obtained by summing up all of the panel forces

$$\bar{F}_{total} = \sum_{ij} \bar{F}_{ij} \tag{9}$$

Aerodynamic wave drag was then the x-component of the resultant aerodynamic force.

The optimization algorithm perturbed each of the Fourier coefficients to obtain a slightly different shape. After perturbing all of the coefficients and analyzing these new perturbed shapes, the optimization algorithm combined the changes into a new shape that met the constraints of constant volume and constant length, but which had a reduced aerodynamic wave drag.

The second part of the study was exactly the same as the first except that instead of working with the Fourier series coefficients we worked with the y and z coordinates of the cross sections' points directly.

Results

Four test cases were run for each part of this study. They consisted of a straight cone having circular cross section shapes, a straight cone having a four pointed star as a cross section, a stubby-wing shaped body and a Space Shuttle-like configuration. All cases were run at an angle of attack of 0°, a specific heat ratio of $\gamma = 1.4$ and a free stream Mach number of $M_\infty = 10$. Notice that the values for γ and M_∞ appear in C_{po} which may be factored out of the pressure coefficient ratio. They affect the numerical amount of drag, but not the qualitative amount of drag. The x-axis for each case was chosen to coincide with the long axis of the body. The y and z-axes were then mutually perpendicular to the x-axis.

Fourier Series Algorithm: For the initial part of the study, twenty terms in a Fourier series for y and z coordinates were used for seven cross sections. Twenty terms were chosen because of the constraints of computational facilities (an IBM 3090 was used) and because twenty terms were able to represent the geometries of all four test cases, including the complex Space Shuttle shape. Only six of the cross sections were allowed to deform; the nose cross section was kept constant to serve as a tip. Thus there were 6 x 20 x 2 = 240 design variables. Twenty-five points were used per cross section; thus, the half body was discretized into 6 x 24 = 144 panels. FAC, the percent perturbation of A_{mi} and B_{mi} in the optimization algortihm, was set equal to 5%.

For the case of a right circular cone (Fig. 2), after a total of 43 iterations, the program converged to an ogive configuration that had 47.96% less wave drag than the original conical configuration. Note that horizontal and vertical symmetry were maintained.

The next shape tested was a four pointed star configuration (Fig. 3). The aerodynamic wave drag of this shape was reduced by 39.16% after 43 iterations. This case did not converge due to "fishtailing" of the fins and was terminated just before such fishtailing occurred. Note the streaking near the nose and the thinning of the points on the last cross section. Also, notice that vertical and horizontal symmetry was maintained and the fins gave an ogiving contour.

The third shape optimized was that of a "stubby wing" configuration (Fig. 4). The wave drag was reduced by 64.62% when the algorithm converged after 53 iterations while preserving the cross-axis symmetry. Again, note the streaking toward the nose and the smooth appearance of four small fins along the wing tip line.

The fourth test case was that of a Space Shuttle configuration (Fig. 5). After 22 iterations, the wing surface crossed itself and the process was terminated. Aerodynamic wave drag was reduced by 18.52%. With careful scrutiny, one can notice that the centerbody has become ogived, the wing thickness has been reduced, the wing roots have become filleted, and the underside of the fuselage has been reduced in size.

The convergence histories (Fig. 6) indicate that the general trend is a monotonic decrease in drag. This trend can also be seen from the drag plot (Fig. 7) which shows the percentage of original drag remaining at a given iteration number (Table 1).

Point-Motion Algorithm: For the point-motion algorithm, 21 points per half cross section were used. Only six cross sections were analyzed due to computer storage limitations. With only five cross sections being active, this yielded 2 x 5 x 21 = 210 design variables and 5 x 20 =100 surface panels per half cross section. FAC for this algorithm was set to 0.1%.

Numerical optimization of a straight circular cone resulted in an ogive shape with axisymmetry successfully maintained. After 49 iterations, the shape converged to that of Fig. 8 with a corresponding decrease in drag of 45.37%.

The second shape was the four pointed star. With the point-motion algorithm, the shape converged after 35 iterations to that pictured in Fig. 8. There was a reduction of drag of 34.65%. As in the case of the circular cone, symmetry was maintained across both the y and z-axes. The resulting shape is very similar to that obtained by the coefficient algorithm. Considerably less streaking can be seen near the nose of the star, while the fin planforms exibited significant ogiving.

The next shape optimized was the "stubby wing". The fin tips, after 24 iterations, crossed themselves and the process was terminated. However, a decrease of 40.58% of the original wave drag was achieved just before the shape cross-over. Note the development of the fins along the side of the vehicle (Fig. 8) and streaks near the nose, somewhat similar to those developed when using the coefficient algorithm. Once again, symmetry was maintained.

The final case for the point motion algorithm was the Space Shuttle vehicle (Fig. 8). Similar to the case in the coefficient algorithm, the wing eventually crossed itself and the run was terminated. A decrease in drag of 27.38% was found after 16 iterations preceding the cross-over.

For the point-motion algorithm, the convergence histories (Fig. 9) indicate monotonic decrease in wave drag for all four test configurations. Figure 10 demonstrates the total reduction in wave drag for the four test configurations when using the point-motion algorithm (Table 2).

A comparison (Figs. 11 and 12) of the numerically optimized ogive shapes with analytically optimal ogives obtained by Sears and Haack and by von Karman [9] demonstrates the reliability and accuracy of the numerical optimization algorithms.

Conclusions

Two procedures, a coefficient algorithm and a point-motion algorithm, for aerodynamically optimizing aribitrarily shaped hypersonic vehicles have been shown to significantly reduce aerodynamic wave drag while keeping the vehicle's volume and length constant. Both formulations are very fast only because a modified Newtonian flow theory was used as the flow field analysis algorithm. These formulations would be very effective as preliminary design tools for unconventional hypersonic vehicles. The point motion algorithm can be used to keep parts of the original vehicle fixed, such as cabin size or wing thickness, during the optimization. More sophisticated flow field solvers that include viscosity and the effects of heat transfer could be substituted in place of the modified Newtonian theory during the final stages of the optimization.

Acknowledgments

The second author would like to thank Penn State's Propulsion Engineering Research Center, the Penn State CFD Studies Program and the ICIDES project for financial support. Many thanks are due to Mr. Florian Sobieczky for his invaluable assistance in producing the graphics for this paper. The authors would like to thank Apple Computer, Inc. for their donated equipment.

References

1. Dulikravich, G. S, Buss, R. N., Strang, E. J. and Lee, S., "Aerodynamic Shape Optimization of Hypersonic Missiles", AIAA Paper 90-3073, Proceedings of the AIAA 8th Applied Aerodynamics Conference, Portland, OR, August 20-22, 1990.
2. Lee, J. and Mason, W. H., "Development of an Efficient Inverse Method for Supersonic and Hypersonic Body Design", AIAA Paper 91-0395, 29th Aerospace Sciences Meeting, Reno, Nevada, January 7-10, 1991.
3. Blankson, I., "Hypersonic Waveriders: State of the Concept", AIAA Paper 91-0529, Reno, NV , Jan. 7-10, 1991.

New York, 1989.
5. Cox, R.N. and Crabtree, L.F., Elements of Hypersonic Aerodynamics, Academic Press, New York, 1965.
6. Geiger, R. E., "Experimental Lift and Drag of a Series of Glide Configurations at Mach Numbers 12.6 and 17.5," Journal of Aerospace Sciences, April 1962, pp. 410-419.
7. Pshenichny, B. N and Danilin, Y. M., Numerical Methods in Extremal Problems, MIR Publishers, Moscow, 1969.
8. Kuo, S. S., Computer Applications of Numerical Methods, Addison-Wesley Publishing Company, Inc., Philippines, 1972.
9. Ashley, H. and Landahl, M., Aerodynamics of Wings and Bodies, Addison-Wesley Publishing Company, Inc., Reading, Massachusetts, 1965.

Coefficient Test Case	Drag Reduction (%)	# of Optimization Cycles	# of Analysis Calls
Cone	47.96	43	10493
Star	39.16	43	10493
Stubby wing	64.62	53	12689
Space Shuttle	18.52	22	5125

Table 1. Drag reduction, number of optimization cycles and analysis calls for the coefficient test cases that uses Fourier series representation.

Point-Motion Test Case	Drag Reduction (%)	# of Optimization Cycles	# of Analysis Calls
Cone	45.37%	49	10273
Star	34.65	35	7277
Stubby wing	40.58	24	4923
Space Shuttle	27.38	16	3211

Table 2. Drag reduction, number of optimization cycles and analysis calls for the point-motion test cases.

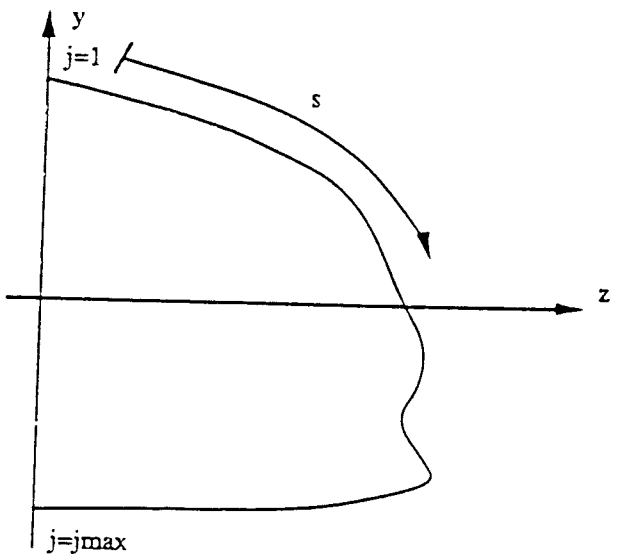

Figure 1. Cross section contour-following coordinate system.

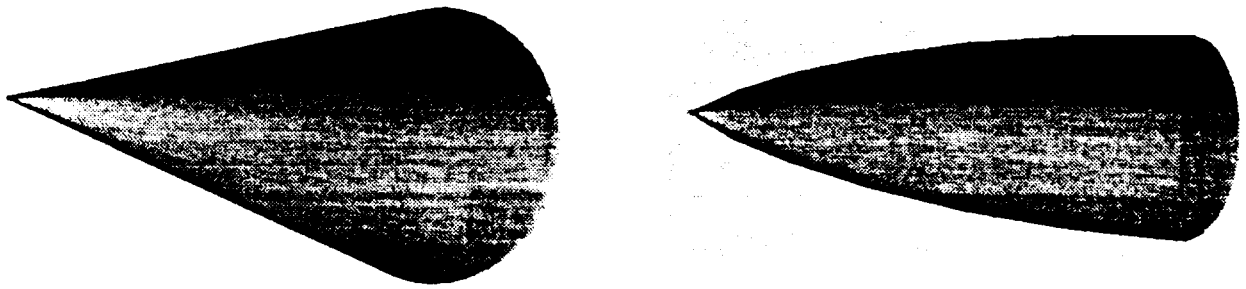

a) initial b) final

Figure 2. Straight circular cone shape; coefficient algorithm: a) initial shape, b) final shape.

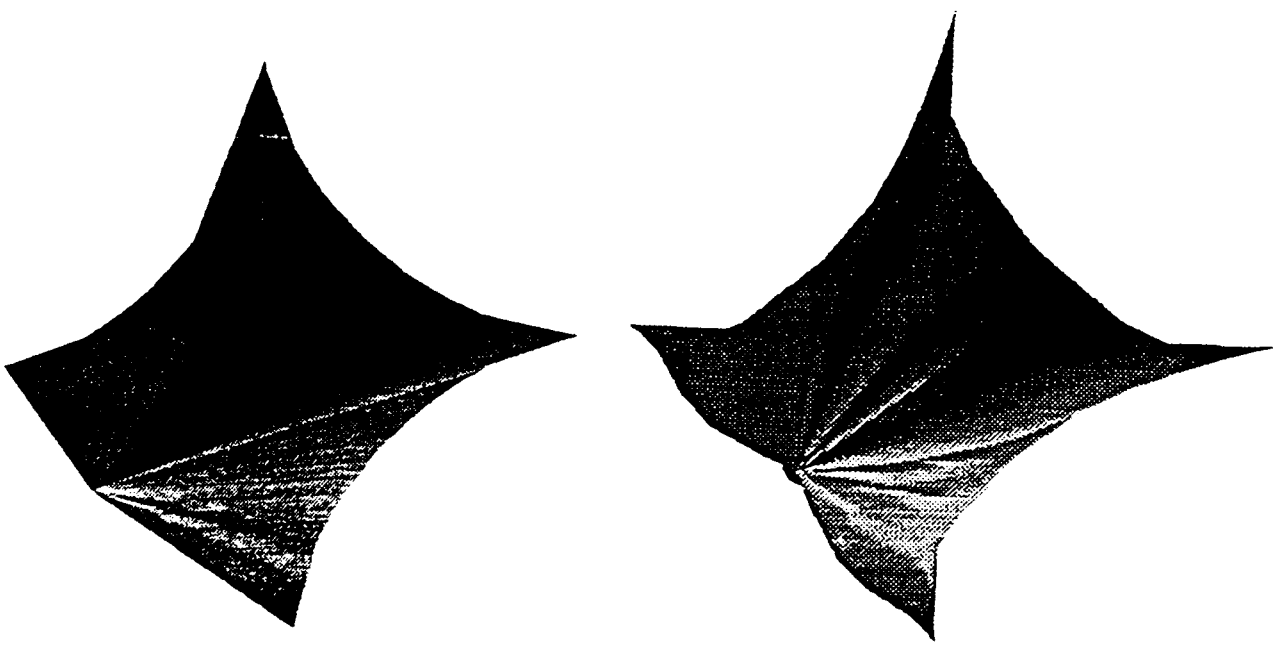

a) initial b) final

Figure 3. Four pointed star shape; coefficient algorithm: a) initial shape, b) final shape.

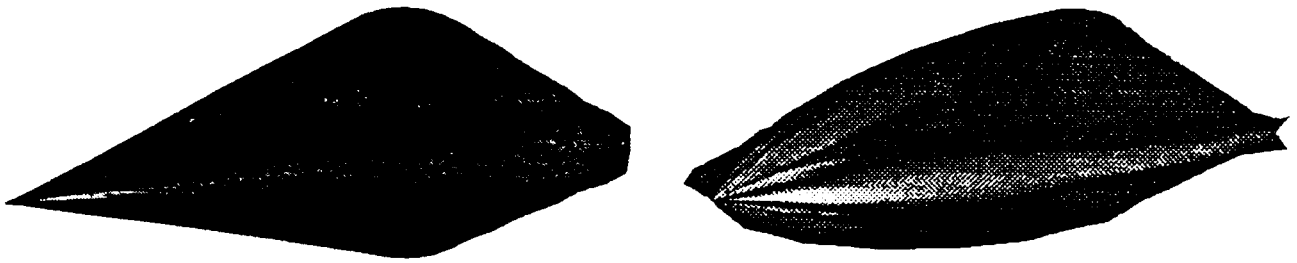

a) initial b) final

Figure 4. Stubby wing shape; coefficient algorithm: a) initial shape, b) final shape.

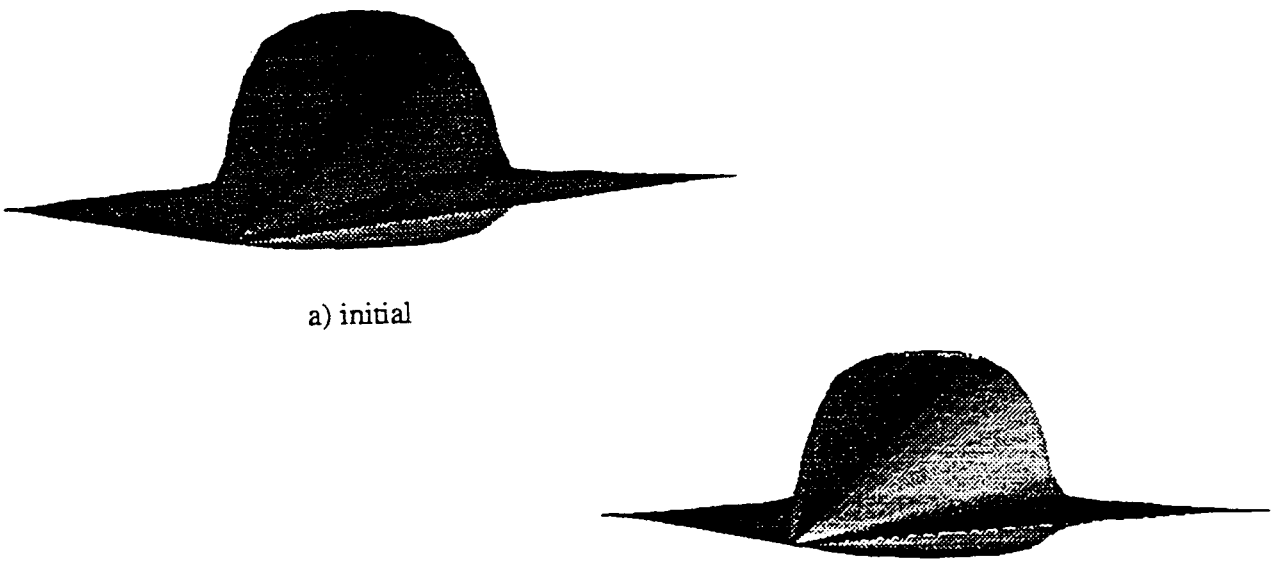

a) initial

b) final

Figure 5. Space Shuttle-like shape; coefficient algorithm: a) initial shape, b) final shape.

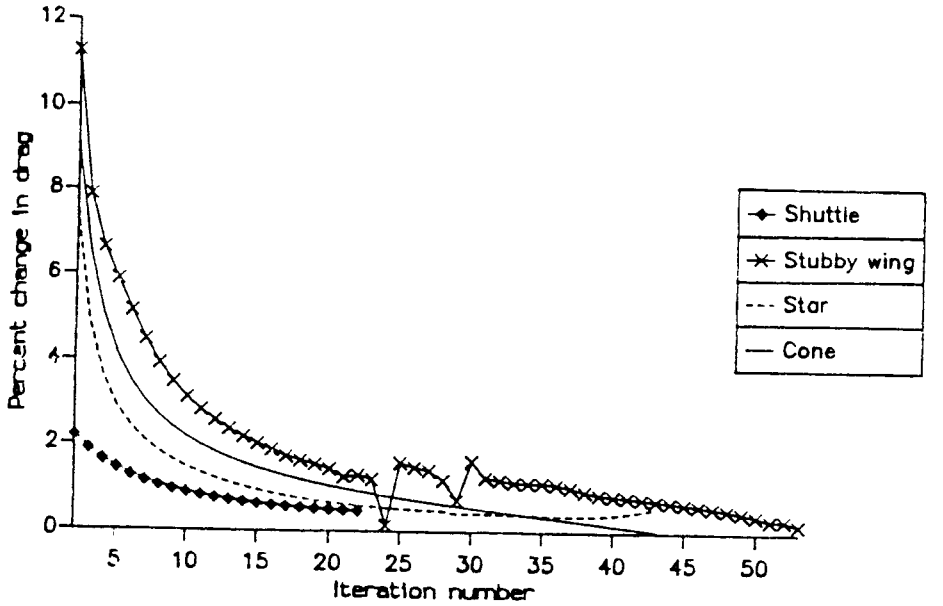

Figure 6. Convergence histories for four test shapes when using coefficient algorithm; percentage change in wave drag per iteration.

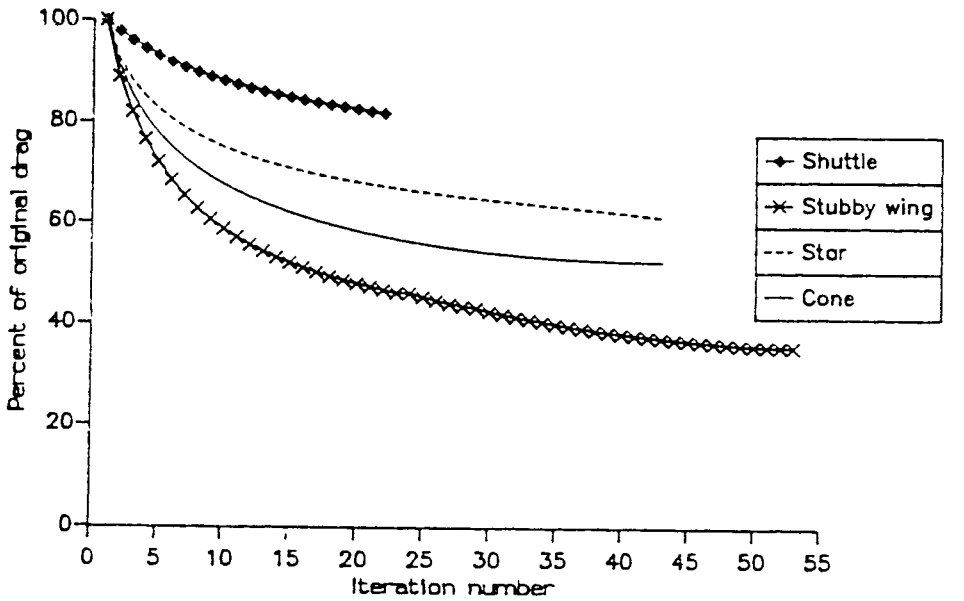

Figure 7. Convergence histories for four test shapes when using coefficient algorithm; total change in wave drag per iteration.

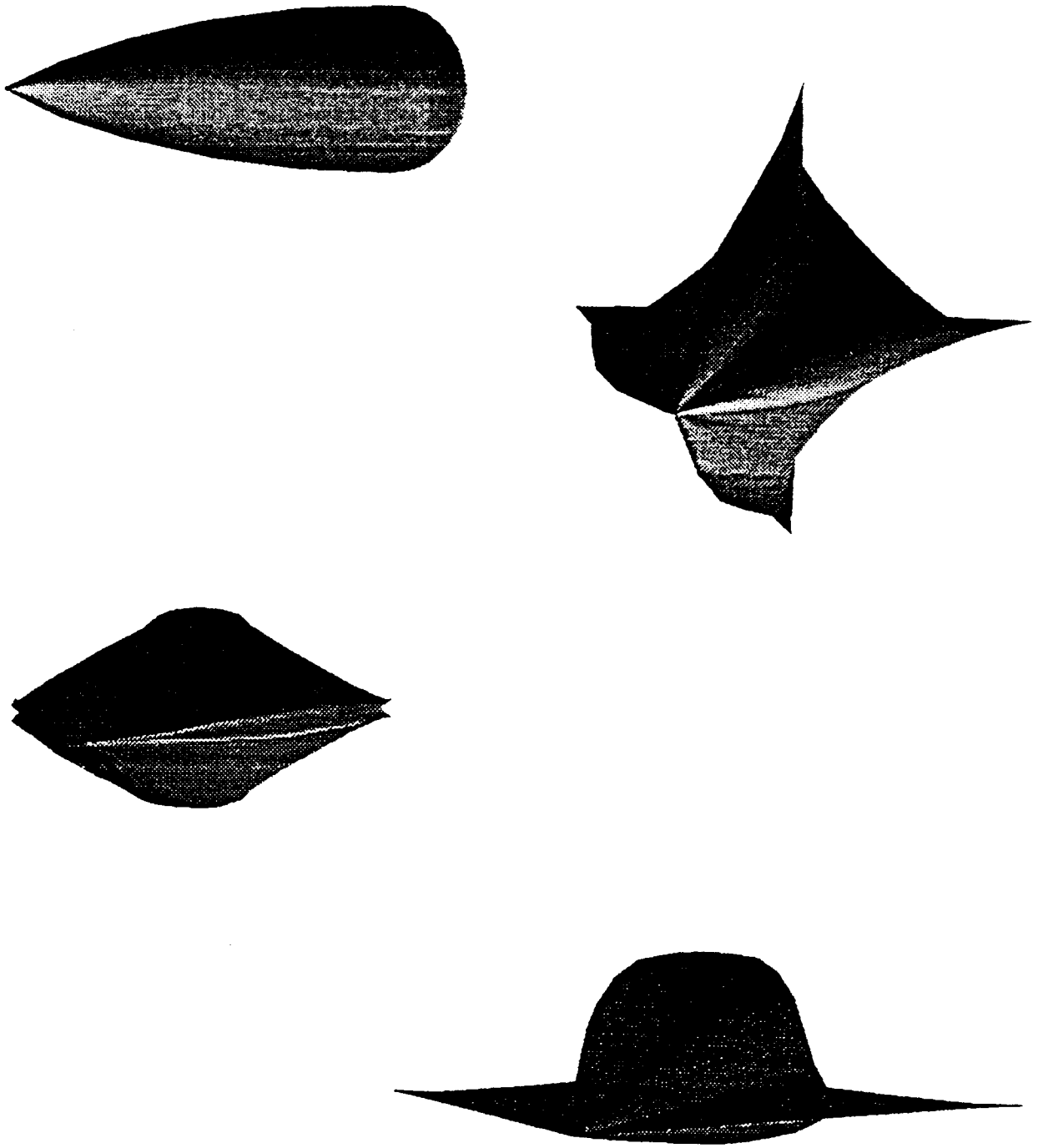

Figure 8. Optimized shapes obtained with the point-motion algorithm.

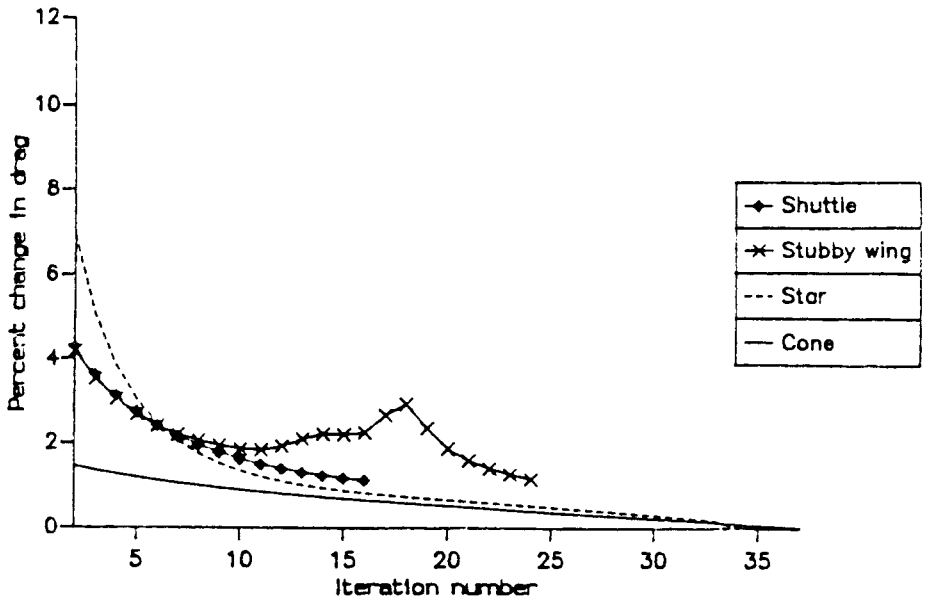

Figure 9. Convergence histories for four test shapes when using point-motion algorithm; percentage change in wave drag per iteration.

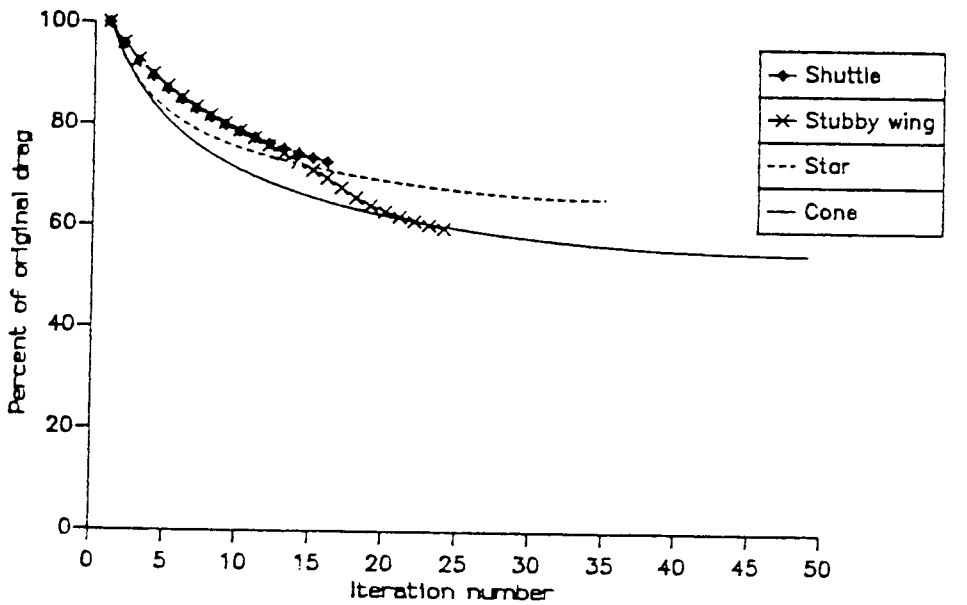

Figure 10. Convergence histories for four test shapes when using point-motion algorithm; total change in wave drag per iteration.

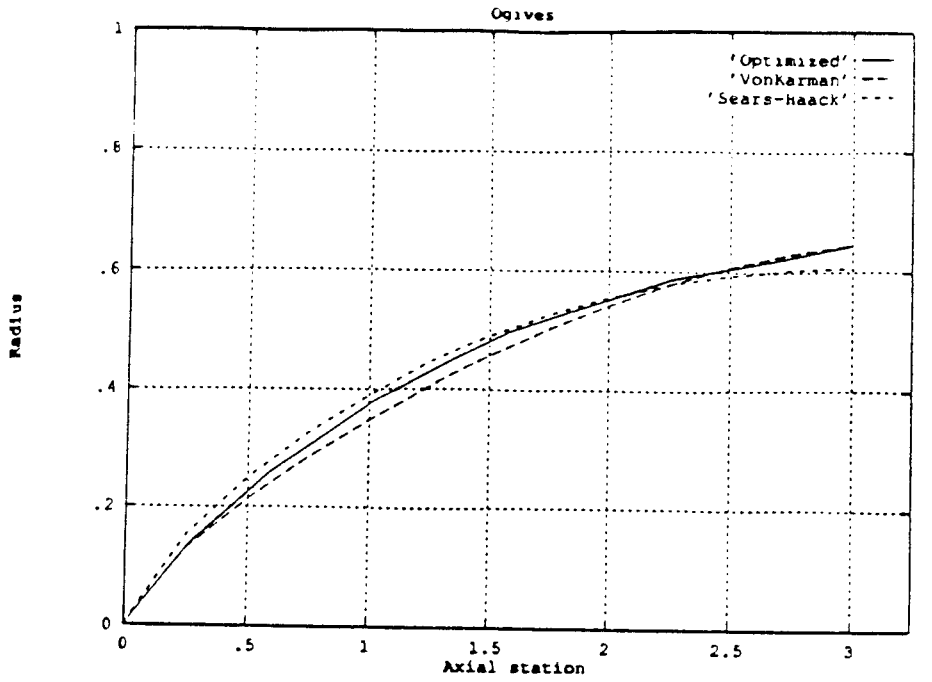

Figure 11. Comparison of analytically optimized ogives and a numerically optimized ogive using coefficient algorithm.

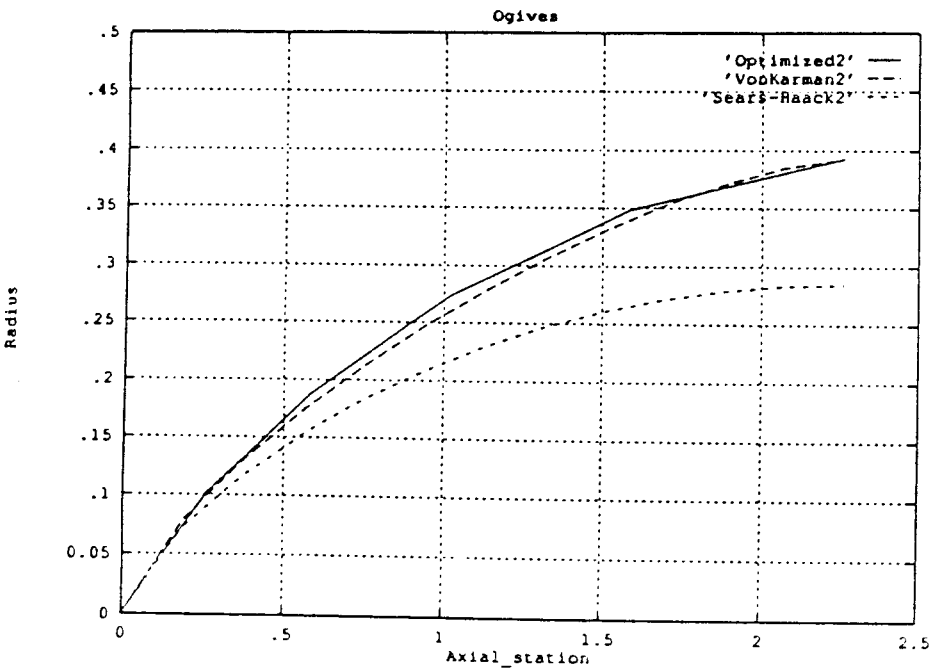

Figure 12. Comparison of analytically optimized ogives and a numerically optimized ogive using point-motion algorithm.